Optics Letters

Characteristics of resonance-induced optical vortices and spatial reshaping

Wei Zhang,[1,*] Aaron Charous,[1] Masaya Nagai,[2] Daniel M. Mittleman,[1] and Rajind Mendis[1,3]

[1]School of Engineering, Brown University, Providence, Rhode Island 02912, USA
[2]Graduate School of Engineering Science, Osaka University, Toyonaka Osaka 560-8531, Japan
[3]Current address: Riverside Research, 2640 Hibiscus Way, Beavercreek, Ohio 45431, USA
*Corresponding author: wei_zhang@brown.edu

Received 26 September 2019; revised 25 October 2019; accepted 26 October 2019; posted 31 October 2019 (Doc. ID 379027); published 27 November 2019

The spatial profile of a beam can experience complicated reshaping after interacting with a planar resonator near resonant conditions. Previously, this phenomenon was recognized as the Goos–Hänchen effect, which only partially explains the experimental observations. In this Letter, we introduce a 2D model that can fully describe the resonance-induced spatial reshaping. The model predicts several general features of the output beam profile and suggests that optical phase or polarization vortices can be generated and manipulated by an arbitrary planar resonator. We validate our theoretical results with experimental measurements using terahertz spectroscopy.

https://doi.org/10.1364/OL.44.005800

In recent years, spatial engineering of optical beams has attracted particular attention and offered new possibilities for sensing [1–3] and computing [4–8]. The simplest implementation of spatial engineering uses the well-known Goos–Hänchen effect, referring to the lateral shift experienced by a laser beam, as it is totally internally reflected from the interface of two media [9]. This effect originates from the fact that different angular components of the beam acquire different phase angles upon total reflection. This phenomenon exists also in systems that exhibit a resonant response, for example, due to a periodic spatial structuring or the excitation of surface plasmons [10–12]. However, unlike the more familiar case of total internal reflection, where the beam experiences only a lateral shift without significant change in the beam shape, the resonance-induced effects are usually accompanied by complicated spatial distortions, including expansion [13,14] and splitting [15–17].

Previously, we introduced a phenomenological model to describe the interaction between a planar resonator and an incident beam of finite size [18]. We showed that there exist two general features in the output spatial profile. First, under certain conditions, the output beam profile is almost identical to the (scaled) incident profile, but laterally shifted, which corresponds to the familiar Goos–Hänchen effect. Second, the output spatial profile always has an exponentially-decaying tail whose decay rate is directly related to the spectral linewidth of the resonance, a signature which can be used for spectroscopic purposes. This earlier model used a 1D approximation and does not take into account the polarization effects, which therefore neglects important aspects of the scattering problem.

In this Letter, we introduce a 2D model that can fully describe the resonance-induced spatial reshaping. The 2D model predicts that a Gaussian beam interacting with a planar resonator generates either a pair of phase vortices with opposite charges ($+1$ and -1) or two pairs of polarization vortices with opposite charges ($+1/2$ and $-1/2$), depending on the incident polarization. These vortices can be manipulated such that they can merge or split as the frequency, incident angle, or polarization is tuned. This result suggests that optical phase and polarization vortices can be created from arbitrary planar resonators, providing an alternative method for generating and manipulating optical vortices, which have important applications in light-matter interaction [19], quantum computing [20], and optical communication [21]. Our experimental results from a terahertz (THz) metallic resonator validate the theoretical predictions. We also show that the 2D model reduces to the 1D model under certain conditions, which is consistent with our earlier conclusions [18].

We consider a planar structure which exhibits a resonant mode that is due, for example, to a periodic geometrical structure [22] or a plasmonic resonance [16]. Commonly, the resonator is polarization dependent; thus, we can decompose the incident field into two orthogonal components, i.e.,

$$\mathbf{E}_{\text{in}}(x, y) = E_{\text{res}}(x, y)\ \mathbf{e}_{\text{res}} + E_{\text{non}}(x, y)\ \mathbf{e}_{\text{non}}, \quad (1)$$

where $\mathbf{e}_{\text{res}}$ and $\mathbf{e}_{\text{non}}$, respectively, are the resonant and non-resonant polarization (normalized and orthogonal) states, and $E_{\text{res}}(x, y)$ and $E_{\text{non}}(x, y)$ are the corresponding complex amplitudes. The resonator has a complicated angular (or k-space) response for the resonant polarization direction ($\mathbf{e}_{\text{res}}$); thus, the corresponding output spatial profile experiences a complicated reshaping. We denote this reshaping using an operator $\hat{H}$. For the non-resonant polarization component ($\mathbf{e}_{\text{non}}$), the angular (or k-space) response of the resonator is nearly

constant; thus, the output spatial profile experiences an almost uniform decay and phase shift, which can be simply described by a complex constant η. As a result, the total output spatial profile can be expressed as

$$\mathbf{E}_{\text{out}}(x, y) = \hat{H} E_{\text{res}}(x, y)\ \mathbf{e}_{\text{res}} + \eta E_{\text{non}}(x, y)\ \mathbf{e}_{\text{non}}. \quad (2)$$

We first discuss the case when the incident beam is aligned with the resonator's polarization, i.e., the second term in Eq. (2) is zero. In this case, we show that a pair of phase vortices with charges $+1$ and -1 can be generated and manipulated in the output beam. We then move to the more general case where the incident beam has arbitrary polarization. In this case, we show that two pairs of polarization vortices with charges $+1/2$ and $-1/2$ can be generated and manipulated in the output beam.

When the incident beam has the same polarization state to the resonant eigenstate $\mathbf{e}_{\text{res}}$, the incident field can be treated as a scalar field, i.e., only the complex amplitudes $E_{\text{res}}(x, y)$ need to be considered. The dispersion relation of the resonant mode depends on the constituent material and geometry of the resonator. The results described here are not restricted to a specific type of dispersion relation. However, for illustrative purposes, we assume that the dispersion relation of the mode has a paraboloidal shape, as in Fig. 1(a). The dispersion relation can be represented as the iso-frequency contours, shown by the gray ellipses in Fig. 1(b). We then consider a monochromatic incident beam with a finite size (in $\mathbf{e}_{\text{res}}$ polarization), whose k-space distribution is illustrated as the blue spot in Fig. 1(b). The monochromatic incident beam can only interact with the iso-frequency contour of the resonator corresponding to the same frequency, which is marked in red. Since the interaction is localized to a small region near the center of the k-space distribution of the incident beam, we can define a new coordinate system (k'_x and k'_y) centered on the incident k-space distribution. In this new coordinate system, the equation of the iso-frequency contour, which defines the resonant condition,

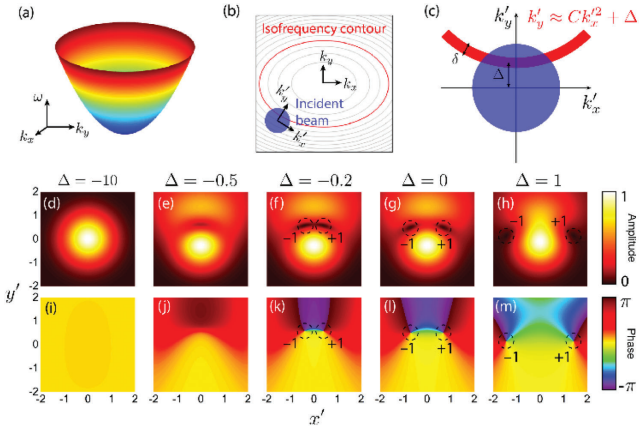

Fig. 1. 2D model describing the resonance-induced spatial reshaping phenomenon when the incident polarization is identical to the resonant polarization. (a) Example dispersion relation of a planar resonator, which has a paraboloidal shape. (b) Iso-frequency contours of the resonator's dispersion relation (gray and red ellipses) and k-space distribution of the incident beam (blue spot). (c) Close-up of (b) with a new coordinate system centered at the middle of the k-space distribution of the incident beam. (d)–(h) Normalized amplitude profiles and (i)–(m) phase profiles of the output beam calculated from the model with different values of the unitless detuning parameter Δ.

can be represented as

$$k'_y = \Delta + \alpha k'_x + C k'^2_x + O\left(k'^3_x\right), \quad (3)$$

where Δ, α, and C, respectively, are the zeroth-, first-, and second-order expansion coefficients, describing the detuning, orientation, and curvature of the dispersion relation. By suitably choosing the orientation of the new coordinate system, α can be set to zero. In addition, we neglect the third- and higher-order terms. Thus, the resonant condition in the new coordinate system can be represented as

$$k'_y \approx \Delta + C k'^2_x, \quad (4)$$

as illustrated in Fig. 1(c). The parameters Δ and C in Eq. (4) have clear physical meanings: Δ represents the detuning from the resonant condition (which could be caused by the offset of either the frequency or the incident angle), and C represents the curvature of the dispersion relation, i.e., the group velocity dispersion of the mode. We further assume very generally that the resonance has a Fano lineshape [23], which has a complex amplitude spectrum given by [24]

$$H\left(k'_x, k'_y\right) = -\frac{1}{1 - iq} + \frac{1}{1 + i\Omega}, \quad (5)$$

where q is the Fano parameter, and Ω is the dimensionless offset from the resonant condition. Since the resonant condition is defined by Eq. (4), Ω can be expressed as

$$\Omega \approx 2\left(k'_y - C \cdot k'^2_x - \Delta\right)/\delta, \quad (6)$$

where δ is the k-space linewidth of the resonance. Then the response of this resonant system can be completely described as

$$H\left(k'_x, k'_y\right) \approx -\frac{1}{1 - iq} + \frac{1}{1 + 2i\left(k'_y - C \cdot k'^2_x - \Delta\right)/\delta}. \quad (7)$$

Equation (7) is a 2D model that describes the resonance-induced spatial reshaping when the incident polarization is identical to the resonant polarization (i.e., the operator $\hat{H}$ mentioned earlier). For any given incident beam whose polarization is aligned with the resonant mode of the resonator, the output spatial profile can be computed by multiplying the incident k-space distribution with Eq. (7), followed by an inverse Fourier transform.

Although the 2D model can be used for any input beam profile, here we consider a specific case which is one of the most common beam profiles: a Gaussian beam, i.e.,

$$E_{\text{res}}\left(x', y'\right) = g_{\text{in}}\left(x', y'\right) = \exp\left(-\frac{x'^2 + y'^2}{w^2}\right), \quad (8)$$

where w is the waist radius. The corresponding k-space distribution can be represented as

$$G_{\text{in}}\left(k'_x, k'_y\right) = \pi w^2 \exp\left(-\frac{k'^2_x + k'^2_y}{(2/w)^2}\right). \quad (9)$$

As a result, the distribution of the output beam in real space can be represented as

$$g_{\text{out}}(x', y') = -\frac{1}{1-iq} g_{\text{in}}(x', y') + \mathcal{F}^{-1}\left\{\frac{\pi w^2 \exp\left[-\left({k'_x}^2 + {k'_y}^2\right)/(2/w)^2\right]}{1 + 2i\left(k'_y - C\cdot {k'_x}^2 - \Delta\right)/\delta}\right\}, \tag{10}$$

where $\mathcal{F}^{-1}$ represents the inverse Fourier transform operator.

Equation (10) can be easily computed numerically. Figures 1(d)–1(m) illustrate several examples of the amplitude and phase profiles of the output spatial distribution from a Gaussian input with different values of Δ and with other parameters set as $q = 0.1 + 0.1i$, $C = 0.3$, $\delta = 2$, and $w = 1$. We observe that, for very negative or very positive values of Δ, the output profile is almost identical to the (scaled) input profile, as in Figs. 1(d) and 1(i). This is because when the incident condition is far from the resonant condition, the resonator has almost no impact on the beam other than attenuation. However, as Δ becomes closer to zero, i.e., the incident condition approaches the resonant condition, the beam profile experiences complicated reshaping: as Δ increases, a dip starts to form near the center of the output beam [Figs. 1(e) and 1(j)]; then two optical vortices with opposite signs (+1 and −1) are generated [Figs. 1(f) and 1(k)]. This vortex pair then splits further, moving continuously away from the region of the beam [Figs. 1(g) and 1(l)]. Finally, the output profile returns to nearly Gaussian [Figs. 1(h) and 1(m)].

Given the condition that the input polarization is aligned with the resonator's polarization direction, the evolving pattern of the output beam profile described above is general, despite the specific properties of the resonator and the Gaussian beam assumed in Fig. 1. This result has a useful practical application—generating optical vortices. Optical vortices can be generated using various optical components such as spiral phase plates, holograms, q-plates, and Gaussian lenses [21,25,26]. However, these devices usually require careful design considerations in the structure. Our theoretical results suggest that optical vortices can be generated in a controllable manner from arbitrary planar resonators, regardless of their detailed structure or design, thus enabling a plethora of possibilities in vortex-generating devices such as plasmonic resonators, photonic crystal slab resonators, and metamaterial resonators [27].

We now discuss the case when the polarization of the incident beam is arbitrary. In this case, generally, there does not exist a point where the field amplitude is completely zero (as in the phase vortex), due to the introduction of the non-resonant polarization component whose field amplitude is always non-zero (unless the incident beam itself has phase vortices). However, under certain conditions, there can exist polarization singularities, where the polarization major axis is undefined, and the field is perfectly circularly polarized (i.e., C-points) [21]. For a field described by $a_1\mathbf{e}_1 + a_2\mathbf{e}_2$, where $\mathbf{e}_1$ and $\mathbf{e}_2$ are normalized and orthogonal polarization states, and a_1 and a_2 are the corresponding complex amplitude, the condition for this field to be circularly polarized is $|a_1| = |a_2|$ and $\arg(a_1) - \arg(a_2) = \beta \pm \pi$, where β is a constant determined by the relative phase between the choice of $\mathbf{e}_1$ and $\mathbf{e}_2$ [21]. In our case, the output field is described by Eq. (2); thus, when the non-resonant polarization component is small, we can always find two points near each phase vortex of the resonant polarization component whose total field is ideally circularly polarized with opposite handedness, corresponding to two C-point polarization vortices with opposite charges (+1/2 and −1/2). Since the phase vortices are generated in pairs, a total of four (or two pairs of) polarization vortices can be generated. When the amplitude of the non-resonant polarization component increases, one pair of polarization vortices merges and annihilates, while the other pair moves to infinity.

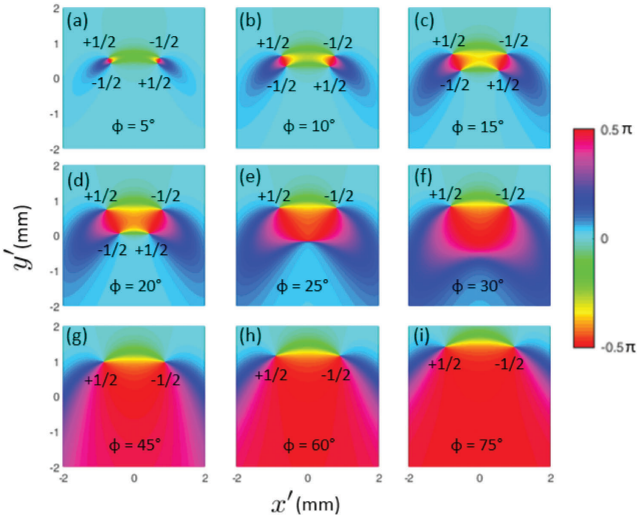

Fig. 2. Generation and evolution of phase vortices from a planar resonator. The resonator has a linearly polarized resonance in x direction with parameters of $q = 0.1 + 0.1i$, $C = 0.3$, $\delta = 2$, and $\Delta = 0$, and is illuminated by a linearly polarized Gaussian beam with a waist radius of $w = 1$ and a polarization orientation of ϕ. (a)–(i) Orientation angle of the polarization major axis of the output beam for various ϕ of the incident beam, ranging from 5° to 75°.

We now show an example on the generation and evolution of the polarization vortices. We consider a resonator with a linearly polarized resonance in x direction with parameters of $q = 0.1 + 0.1i$, $C = 0.3$, $\delta = 2$, and $\Delta = 0$, illuminated by a linearly polarized Gaussian beam with a waist radius of $w = 1$. If the incident beam is polarized in x direction, the output beam has a spatial profile, as shown in Fig. 1(g) (amplitude) and Fig. 1(l) (phase). However, we now consider that the incident beam is polarized at an angle ϕ to the x-axis. In this case, the output spatial profile is elliptically polarized in general. Figure 2 illustrates the orientation angle of the polarization major axis of the output beam for various ϕ of the incident beam, ranging from 5° to 75°. We observe that, when $\phi = 5°$ (i.e., the non-resonant polarization component is small), two pairs of polarization vortices with charges +1/2 and −1/2 appear in the output beam [Fig. 2(a)], near the position of the phase vortices in the resonant polarization component [Figs. 1(g) and 1(l)]. As ϕ increases (i.e., the amplitude of the non-resonant polarization increases), two of the four polarization vortices merge and annihilate, while the other two move to infinity.

We also demonstrate that the 1D model discussed earlier [18] can be derived from this 2D model [Eq. (7)] in the case that the input polarization is aligned with the resonator's polarization direction. We consider two circumstances to reduce the dimension from 2D to 1D. The first circumstance is when the device has a linear dispersion. In this case, parameter C is equal to zero, and the model becomes equivalent to that discussed in Ref. [18]. The second circumstance is when the measurement is

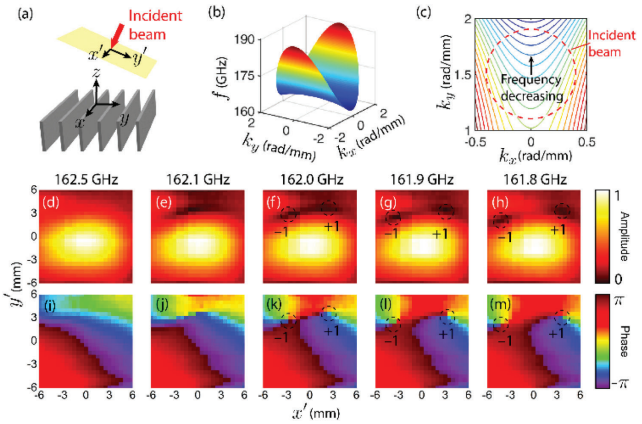

Fig. 3. Experimental validation of the 2D model. (a) THz planar resonator made by a periodic array of thin metal plates is illuminated by a THz Gaussian beam. (b) Simulated dispersion relation of the resonant mode of the device. (c) Simulated iso-frequency contours (solid curves) and incident beam k-space distribution (dashed curve) of the dispersion relation. As the frequency decreases, the iso-frequency contour shifts upward, corresponding to an increasing unitless detuning parameter. (d)–(h) Measured normalized amplitude profiles and (i)–(m) phase profiles of the transmitted beam for different values of the incident frequency.

performed in 1D, i.e., x direction is averaged during the measurements (using, for example, a slit aperture). In this case, we measure only the $k'_x = 0$ component, and Eq. (5) once again becomes equivalent to that in Ref. [18].

To validate our theoretical results, we perform experimental measurements on a planar resonator, designed to exhibit narrow resonances at THz frequencies. The resonator consists of a periodic array of thin metal plates, with a plate separation of 1 mm, a plate thickness of 0.1 mm, and a plate width of 4 mm, as illustrated in Fig. 3(a). We have previously shown [22] that this structure exhibits several resonances in the THz range. Here we focus on the resonance near 0.162 THz. We simulate the dispersion relation [Fig. 3(b)] and the iso-frequency contours [Fig. 3(c)] of this resonant mode using the finite-element method. We illuminate the device with a p-polarized broadband Gaussian beam with a $1/e$ beam diameter of 10 mm, and we measure the amplitude [Figs. 3(d)–3(h)] and phase [Figs. 3(i)–3(m)] of the transmitted beam using THz time-domain spectroscopy. We observe that, at 162.5 THz (off-resonance), the output beam is approximately Gaussian, almost identical to the incident beam. However, as the frequency decreases (corresponding to an increase in Δ from negative values towards positive values), two optical vortices with opposite charges ($+1$ and -1) are generated. These two vortices split and move exactly as predicted by the model described above.

In conclusion, we introduce a 2D model that describes resonance-induced spatial reshaping phenomena. Our model suggests that an optical phase and polarization vortices can be generated and manipulated using an arbitrary planar resonator, providing an alternative method for generating optical vortices. The model can be reduced to 1D under certain conditions, thus demonstrating consistency with our earlier work [18]. We compare our theoretical results with experimental measurements at THz frequencies and find excellent agreement.

Funding. National Science Foundation.

Acknowledgment. The authors are grateful for useful discussions with Prof. Chia Wei Hsu.

REFERENCES

1. T. Hashimoto and T. Yoshino, Opt. Lett. **14**, 913 (1989).
2. X. Yin and L. Hesselink, Appl. Phys. Lett. **89**, 261108 (2006).
3. T. Shui, W.-X. Yang, Q. Zhang, X. Liu, and L. Li, Phys. Rev. A **99**, 013806 (2019).
4. A. Silva, F. Monticone, G. Castaldi, V. Galdi, A. Alù, and N. Engheta, Science **343**, 160 (2014).
5. L. L. Doskolovich, D. A. Bykov, E. A. Bezus, and V. A. Soifer, Opt. Lett. **39**, 1278 (2014).
6. Z. Ruan, Opt. Lett. **40**, 601 (2015).
7. T. Zhu, Y. Zhou, Y. Lou, H. Ye, M. Qiu, Z. Ruan, and S. Fan, Nat. Commun. **8**, 15391 (2017).
8. T. Zhu, Y. Lou, Y. Zhou, J. Zhang, J. Huang, Y. Li, H. Luo, S. Wen, S. Zhu, Q. Gong, M. Qiu, and Z. Ruan, Phys. Rev. Appl. **11**, 034043 (2019).
9. F. Goos and H. Hänchen, Ann. Phys. **436**, 333 (1947).
10. L.-G. Wang and S.-Y. Zhu, Opt. Lett. **31**, 101 (2006).
11. J. Hao, H. Li, C. Yin, and Z. Cao, J. Opt. Soc. Am. B **27**, 1305 (2010).
12. P. Ma and L. Gao, Opt. Express **25**, 9676 (2017).
13. Y. Wan, Z. Zheng, W. Kong, X. Zhao, and J. Liu, IEEE Photonics J. **5**, 7200107 (2013).
14. Y. Fan, N. Shen, F. Zhang, Z. Wei, H. Li, Q. Zhao, Q. Fu, P. Zhang, T. Koschny, and C. M. Soukoulis, Adv. Opt. Mater. **4**, 1824 (2016).
15. I. V. Shadrivov, A. A. Zharov, and Y. S. Kivshar, Appl. Phys. Lett. **83**, 2713 (2003).
16. P. Xiao, J. Opt. Soc. Am. B **28**, 1895 (2011).
17. I. V. Soboleva, V. V. Moskalenko, and A. A. Fedyanin, Phys. Rev. Lett. **108**, 123901 (2012).
18. W. Zhang, A. Charous, M. Nagai, D. M. Mittleman, and R. Mendis, Optica **5**, 1414 (2018).
19. M. Babiker, D. L. Andrews, and V. E. Lembessis, J. Opt. **21**, 013001 (2019).
20. M. Erhard, R. Fickler, M. Krenn, and A. Zeilinger, Light Sci. Appl. **7**, 17146 (2018).
21. G. J. Gbur, *Singular Optics* (CRC Press, 2016).
22. W. Zhang, A. Charous, M. Nagai, D. M. Mittleman, and R. Mendis, Opt. Express **26**, 13195 (2018).
23. M. F. Limonov, M. V. Rybin, A. N. Poddubny, and Y. S. Kivshar, Nat. Photonics **11**, 543 (2017).
24. M. J. Theisen and T. G. Brown, J. Mod. Opt. **62**, 244 (2015).
25. A. Rubano, F. Cardano, B. Piccirillo, and L. Marrucci, J. Opt. Soc. Am. B **36**, D70 (2019).
26. L. V. Kreminskaya, M. S. Soskin, and A. I. Khizhnyak, Opt. Commun. **145**, 377 (1998).
27. X. Wang, Z. Nie, Y. Liang, J. Wang, T. Li, and B. Jia, Nanophotonics **7**, 1533 (2018).